Analyzing the Shape and Motion of the Lungs and Heart in Dynamic Pulmonary Imaging

Jianming Liang, Tim McInerney and Demetri Terzopoulos

Abstract The "Dynamic Chest Image Analysis" project aims to show focal and general abnormalities of lung ventilation and perfusion based on a sequence of digital chest fluoroscopy frames. An indispensable source of information recorded in the image sequence is the shapes and motions of the lungs and heart. This chapter employs this shape and motion information of lung and heart to detect abnormalities in both lung ventilation and perfusion. To extract the shape and motion information of lung and heart, we utilize a technique, called United Snakes, in which both the shape and motion of the lung and heart can be modeled using a single consistent theoretical and implementational framework. Along with case studies, we demonstrate the capability of United Snakes through four applications: lung registration, diaphragm motion analysis, cardiac motion analysis, and cardiac shape analysis, in revealing both lung ventilation and perfusion abnormalities.

1 Introduction

The respiratory system facilitates the exchange of gases (O_2 and CO_2) between the blood and ambient air; therefore, adequate pulmonary ventilation (air flow) and perfusion (blood flow) are essential for the lungs to function properly. Inadequate pulmonary function may be due to failure in ventilation and perfusion, among other

J. Liang (✉)
Department of Biomedical Informatics, Arizona State University, Scottsdale , AZ 85254, USA
e-mail: jianming.liang@computer.org

T. McInerney
Department of Computer Science, Ryerson University, Toronto, ON, Canada
e-mail: tmcinern@scs.ryerson.ca

D. Terzopoulos
Computer Science Department, University of California, Los Angeles, CA 90095, USA
e-mail: dt@cs.ucla.edu

S. Li and J. M. R. S. Tavares (eds.), *Shape Analysis in Medical Image Analysis*,
Lecture Notes in Computational Vision and Biomechanics 14,
DOI: 10.1007/978-3-319-03813-1_9,

factors. To detect abnormalities of lung ventilation and perfusion, ventilation and perfusion isotope scans are conventionally used, but they can only provide a static, coarse 2D distribution of air and blood in the lungs, and also have a disadvantage of using radioactive isotopes. The primary imaging modality for diagnosing pulmonary disorders is chest X-ray, but the information about pulmonary function (ventilation and perfusion) that may be gleaned from a single chest X-ray is rather limited. To overcome this limitation, this chapter utilizes sequences of digital chest fluoroscopy frames to reveal focal and general pulmonary functional abnormalities by analyzing shape and motion of the lungs and heart.

2 Dynamic Pulmonary Imaging

2.1 Patient Examination

With Dynamic Pulmonary Imaging [1], we can collect a sequence of chest X-ray images of up to 512 × 512 pixels at a sampling frequency of 25 Hz with a copper filter of 3 mm. The reason of using a copper filter is to reduce the radiation dose to patients. Two separate examination procedures are used for ventilation and perfusion studies. In the ventilation study, the patient is asked to breathe naturally and normally in a supine position with posteroanterior projection. An image sequence of 55 frames with 192 × 144 pixels is collected in 4.32 s with a sampling frequency of 12.5 Hz, because in most cases the lungs can complete a full ventilation cycle in 4 s. Based on our experiments, a spatial resolution of 192 × 144 is sufficient for ventilation analysis. In the perfusion study, the patient is also in a supine position with posteroanterior projection, but with breath held to effectively remove the ventilation effects. An intravenous bolus of X-ray contrast medium may be further used to enhance the perfusion signal strength. Comparing with ventilation, perfusion has a higher frequency, thus requiring a higher temporal sampling rate but a shorter examination time. Furthermore, pulmonary perfusion is asynchronous,[1] demanding a higher spatial resolution. As a result, for perfusion analysis we acquire an image sequence of 52 frames with 384 × 288 pixels at a sampling frequency of 25 Hz in 2.04 s. The imaging parameters are summarized in Table 1.

The acquired image sequences may be represented with intensity function $I(x, y, t)$, where $0 \leq I \leq 255, 1 \leq x \leq$ width (192 for ventilation and 384 for perfusion), $1 \leq y \leq$ height (144 for ventilation and 288 for perfusion), and t is a discrete time point in $0 \leq t \leq$ *examtime* (4.32 s for ventilation and 2.04 s for perfusion). We may also represent it as $I(x, y, i)$, with i the frame index, such that $t = (i-1)/f$, where f is the sampling frequency of 12.5 Hz for ventilation analysis and 25 Hz for perfusion analysis.

[1] The speed of blood flow is roughly 10 cm/s. When the blood flows in the lungs, the phase (i.e., timeshifts) of a pulse signal at one location may be different from that at another location, although they have the same pulse frequency.

Table 1 Dynamic pulmonary imaging parameters used for ventilation and perfusion examinations

Examination	Image size	Temporal sampling frequency (Hz)	Number of frames	Examination time (s)
Ventilation	$\geq 192 \times 144$	12.5	55	4.32
Perfusion	$\geq 384 \times 288$	25	52	2.04

Because of the very short examination time and the use of a copper filter, the radiation dose to the patient is low. The entrance skin dose of a patient is about 0.1 to 0.2 mGy [1]. For comparison, the radiation dose of a normal chest X-ray image varies between 0.1 and 0.2 mGy, and the radiation dose of fluoroscopy is about 2 mGy per minute [1].

2.2 Ventilation and Perfusion Analysis

The 2D image sequence obtained from the patient examination carries valuable information for ventilation and perfusion studies thanks to the physical properties of X-rays: The attenuation of X-rays in air is much lower than in blood and soft tissue. As a result, the average pixel intensity of an area in the lung field varies over time due to the respiratory and cardiac cycles; this variation, called a lung functional signal, reflects the air and blood volume change in the corresponding 2D projectional area of the lung when the patient breathes naturally. When the patient is asked to hold their breath, we observe the perfusion signal disturbed by noise. The ventilation intensity variation depends on the depth of the tidal volume ventilation and on lung area. It is usually between 5 and 15 units in the 8-bit grey scale. The image intensity variation for perfusion is about 3 to 4 units without contrast media. The ventilation signal to noise ratio is about 10:1 and the perfusion signal to noise ratio is about 3:1. This phenomenon is illustrated in Figs. 1, 2 and 3.

We detect ventilation and perfusion abnormalities by extracting meaningful ventilation and perfusion parameters from the lung functional signals. To do so, it is necessary to accurately locate the "turning points" from the signal, but it is challenging due to the existence of both ventilation and perfusion components, in addition to noise. Furthermore, a phase (exhalation, inhalation, diastole, or systole) might not be complete in a signal. For instance, the signal in Fig. 1b does not have a complete exhaling phase. To this end, we introduce a mathematical function (Fig. 4):

$$M(A, D, U, S, L, t) = \begin{cases} A\cos(\pi t'/D) + L & \text{if } 0 \leq t' < D \\ A\cos(\pi(t' - D)/U + \pi) + L & \text{if } D \leq t' < (D + U) \end{cases} \quad (1)$$

where

$$t' = (t - S) \mod (D + U), \quad (2)$$

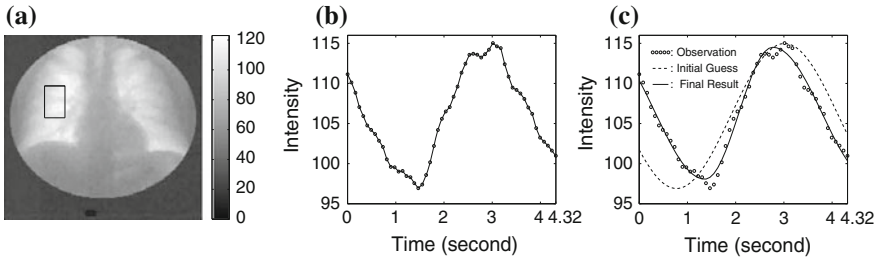

Fig. 1 A case in quiet breath. **a** A region of interest (ROI) in the right lung field and **b** its corresponding lung functional signal (observation), which reflects the air and blood change in the corresponding lung area over time during the examination due to the physical properties of X-rays. **c** A set of ventilation parameters can be extracted from the observation **b** with a ventilation model (see Fig. 4) via optimization, where the observation is indicated with an "o", the initial guess is plotted as a dashed curve and the final solution as a solid curve. The image gets whiter (higher intensity) during inhalation (more air in the lungs). The ROI shown here is a rectangle, but it may be of arbitrary shape. The ROI may be as large as a whole lung or may be as small as a single pixel

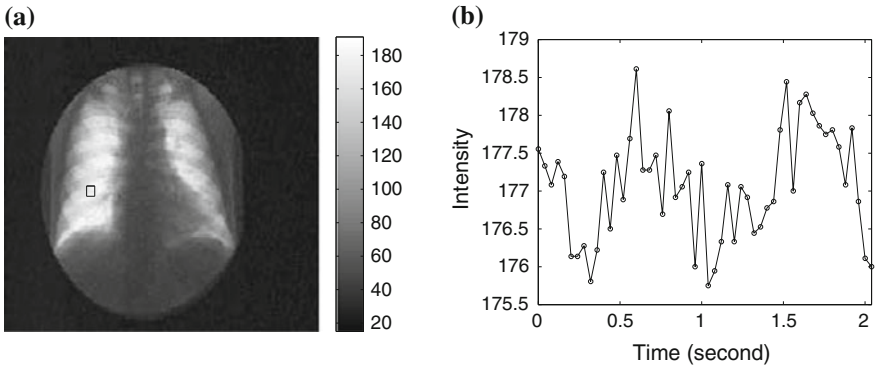

Fig. 2 A case with the breath held and an intravenous bolus of X-ray contrast media. **a** An ROI (region of interest) in the right lung field and **b** its corresponding observation—an enhanced lung perfusion signal which (due to the physical properties of X-rays) reflects the blood flow in the corresponding lung area with contrast media. The image gets darker (lower intensity) during the systolic phase (more blood in the lungs). Comparing to ventilation in Fig. 1, the perfusion signal is very noisy and weak (only about 3 intensity-unit variation)

with t for $time$, and $t' \in [0, D + U)$, so that ventilation and perfusion parameters can be extracted automatically from lung functional signals via optimization [2–4]. From these five extracted parameters, more parameters can be derived. In case of ventilation, we can compute:

- *Ventilation Frequency* ($\hat{F}_v$) (expressed as the number of breaths per minute):

$$\hat{F}_v = 60/(\hat{D}_v + \hat{U}_v), \tag{3}$$

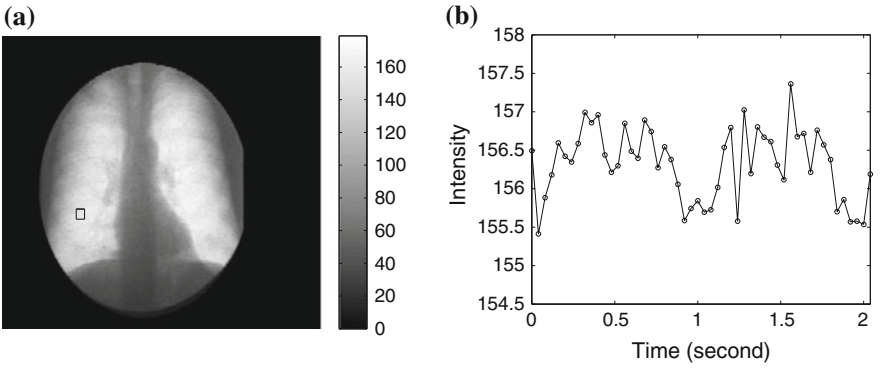

Fig. 3 A case with the breath held but using no X-ray contrast media. **a** An ROI (region of interest) in the right lung and **b** its corresponding observation—a perfusion signal reflecting the blood flow in the lung area due to the physical properties of X-rays. It is plotted in the same scale as in Fig. 2 for comparison

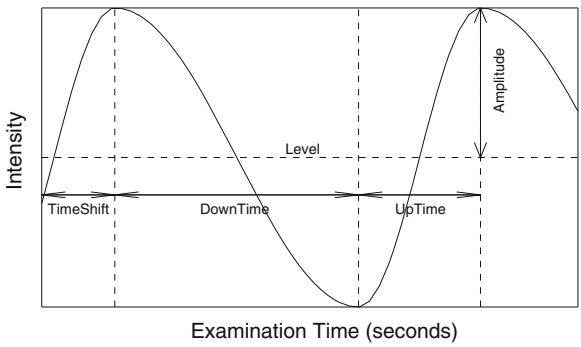

Fig. 4 A mathematical function can be used for both ventolation and perfusion analysis. In case of ventilation, it models the volume change of air during lung ventilation (increasing during inhalation and decreasing during exhalation) with five primitive parameters: *amplitude A* (ventilation strength), *downtime D* (time for exhalation), *uptime U* (time for inhalation), *timeshift S* (time from the starting of examination to the completion of the first inhalation) and *level L* (mean intensity; its value depending on various factors, medical meaning un-defined). In case of perfusion, it models the blood volume change, increasing during the diastolic phase and decreasing during the systolic phase, but its five free primitive parameters have completely different medical meanings: *amplitude A* (perfusion strength in the lung area), *downtime D* (time for the systolic phase in the lung area), *uptime U* (time for the diastolic phase in the lung area), *timeshift S* (time from the first image to the completion of the first diastolic phase) and *level L* (the mean intensity but with no well-defined medical meaning)

- *Inhaling Rate* ($\hat{I}_v$):

$$\hat{I}_v = \hat{A}_v / \hat{U}_v, \tag{4}$$

- *Exhaling Rate* ($\hat{E}_v$):

$$\hat{E}_v = \hat{A}_v / \hat{D}_v, \tag{5}$$

- *Normalized timeshift* ($\hat{H}_v$):

$$\hat{H}_v = \hat{S}_v / (\hat{U}_v + \hat{D}_v), \tag{6}$$

- *Updown Ratio* ($\hat{R}_v$):

$$\hat{R}_v = \log_{10}(\hat{U}_v / \hat{D}_v). \tag{7}$$

We take the logarithm of the "updown ratio" to make it symmetric. All these parameters may be used as ventilation abnormality indicators, but our experiments show that in most cases three parameters, $\hat{A}_v$ (amplitude), $\hat{H}_v$ (normalized timeshift) and $\hat{R}_v$ (updown ratio) are sufficient in revealing ventilation abnormalities.

2.3 Shape and Motion Analysis

An additional, indispensable source of information recorded in the image sequence is the shape and motion of the lungs and heart. This chapter employs this shape and motion information to detect abnormalities of the lungs and heart with the United Snakes technique, which is to be reviewed in Sect. 3. It should be noted that the tasks of lung registration and cardiac motion analysis are challenging, because of the reduced image contrast by the copper filter used in image acquisition to reduce the radiation dose to patients.

3 United Snakes

A snake [5] is a flexible, elastic contour whose behavior is governed by an energy functional, where an internal energy controls the degree of stretchiness and flexibility of the contour while an external energy couples the contour to an image, attracting the snake to features of interest (e.g., intensity edges). The active research in Snakes has resulted in a large family of Snakes algorithms [6–8], including finite element Snakes, B-Snakes, and Fourier Snakes, and related algorithms, such as "live-wire" (also known as "intelligent scissors") [9–15]. Each of these variants has its strengths and weaknesses.

To extract and model the shape and motion of both the lung and the heart in an accurate and robust manner, the differences between these two organs must be taken into consideration and the most appropriate Snake algorithm selected. For example, the lung boundary is smooth with readily identifiable curved corner regions. Consequently, a Hermite finite-element Snake, which can be constructed directly from user-defined lung boundary points and which can easily control the relative position of its nodal points, is most suitable for lung registration and motion analysis. On the other hand, much of the heart boundary is not visible in the image sequence

and there are no readily identifiable landmark points directly on the boundary. In this case, the reduced number of degrees of freedom, high degree of smoothness and control polygon of a B-spline Snake make it an ideal choice. Furthermore, the live-wire algorithm is effective for providing a quick delineation of the lungs and heart and this delineation can then be used by a Snakes algorithm for subsequent segmentation and motion tracking of an image sequence. As a result, a common framework combining the best features of the various Snakes algorithms and the live-wire algorithm is highly desirable.

To this end, United Snakes unifies various Snakes algorithms in a finite element framework, where a particular type of Snake can be derived simply by changing the shape functions at the user level. This unification expands the range of object modeling capabilities within a uniform Snake construction process and provides a uniform Snakes motion tracking mechanism. Consequently, both the shape and motion of the lung and heart can be modeled using a single consistent theoretical and implementational framework. United Snakes is also advantageously combined with live-wire by introducing an effective hard constraint mechanism. The United Snakes framework amplifies the efficiency and reproducibility of the component techniques, and it offers more flexible interactive control while further minimizing user interactions. The reader is referred to [16] for the mathematical details.

In the following sections, along with case studies, we present four applications of United Snakes: lung registration, diaphragm motion analysis, cardiac motion analysis, and cardiac shape analysis.

4 Lung Registration

Through our clinical studies, our expert radiologists have found it convenient and effective to use four rectangles (regions of interests, ROIs) covering the apex, upper, middle and lower lung field in each lung for a quick ventilation examination by inspecting the behaviors of the four corresponding lung functional signals. To facilitate this inspection, we propose an ROI-based analysis with lung registration and division.

4.1 Quick ROI-Based Analysis with Lung Registration and Division

The rapid ROI-based analysis is performed by first interactively delineating the lungs in the first frame with United Snakes (see Fig. 5), and then using the tracking capabilities of Snakes to automatically follow the motion throughout the entire image sequence (Fig. 6). The result is a lung delineation in each frame of the sequence. This step is followed by an automatic division of each lung field into four rectangular regions in each frame (Fig. 7) and an automatic calculation of the average intensity for each region. This process forms four lung functional signals in each lung field, from which ventilation parameters can be automatically extracted as shown in Fig. 8.

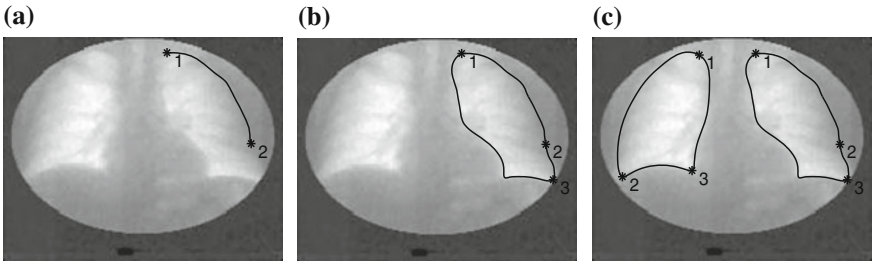

Fig. 5 Lung delineation with United Snakes. Once the first seed (point *1* in (**a**)) is placed on the lung boundary, an interactive snake is automatically constructed from the first seed to the current mouse position (position *2* in (**a**)). With three seeds, the left lung can be delineated (**b**), and similarly for the right lung (**c**)

4.2 Clinical Case Studies

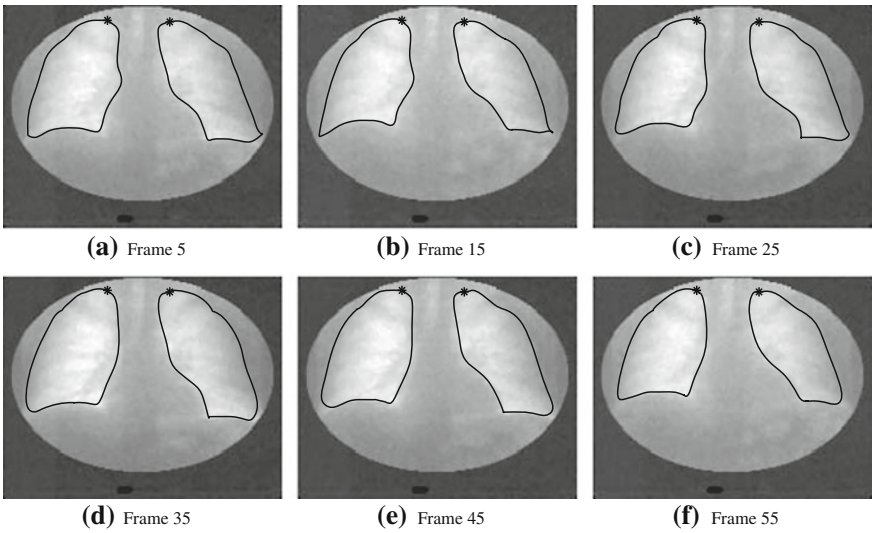

Fig. 6 The tracking result (every tenth image shown). The edge information at the lung apex is rather weak. Furthermore, there is no observable lung motion during quiet breathing. In order to make the snake firmly stick to the apex, it is desirable to maintain a hard constraint point there. Therefore, in the lung delineation as illustrated in Fig. 5, the first seed is usually placed at the lung apex so that it can be utilized as a hard constraint in the tracking process

Here we present two representative cases—one normal and one abnormal—to illustrate typical abnormalities:

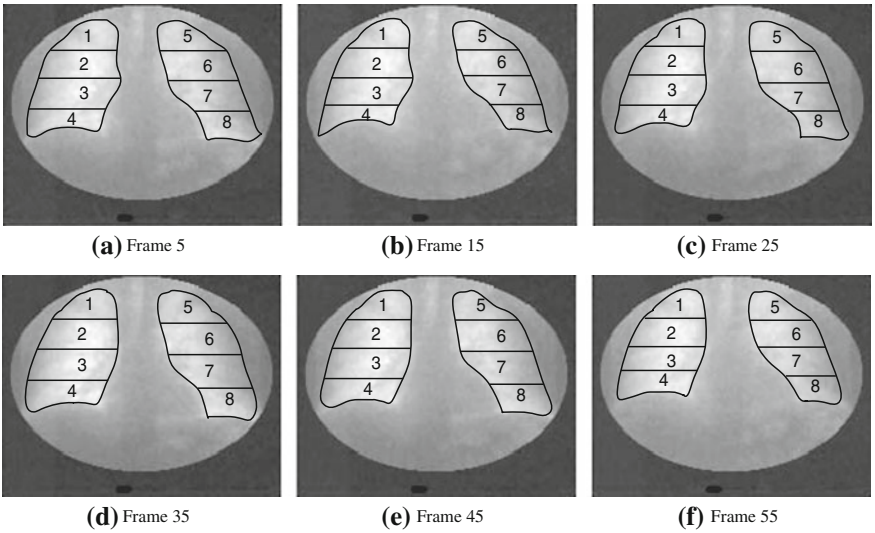

(a) Frame 5 **(b)** Frame 15 **(c)** Frame 25

(d) Frame 35 **(e)** Frame 45 **(f)** Frame 55

Fig. 7 Each lung field is divided into four regions with equal heights in each frame so that four lung functional signals in each lung field can be formed. Ventilation parameters are automatically extracted from these signals (see Fig. 8 and Table 2)

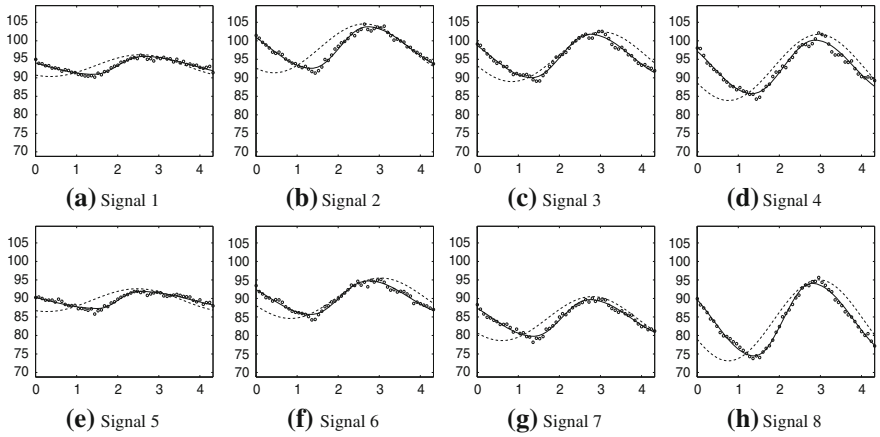

(a) Signal 1 **(b)** Signal 2 **(c)** Signal 3 **(d)** Signal 4

(e) Signal 5 **(f)** Signal 6 **(g)** Signal 7 **(h)** Signal 8

Fig. 8 Extracting the ventilation parameters from the eight lung functional signals resulting from the lung division (the observations are indicated with "o", the initial guesses with dashed curves and the final results with solid curves). The numerical results are given in Table 2

- Case 1: This case has been clinically classified as normal, but we have found some slightly asynchronous ventilation and non-symmetrical ventilation at both apices (see Table 2).

Table 2 Clinical case I: Extracted ventilation parameters

Signal	A	H	R
1	2.43	0.72	−0.325
2	5.61	0.79	−0.186
3	5.87	0.79	−0.160
4	7.23	0.83	−0.099
5	2.32	0.70	−0.421
6	4.54	0.80	−0.174
7	4.95	0.81	−0.181
8	9.79	0.81	−0.169

Clinically normal but slightly asynchronous ventilation (ASV) and non-symmetrical ventilation (NSV) seen in regions 1 and 5

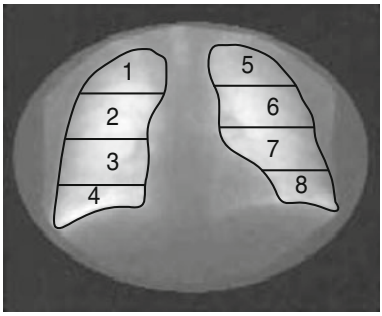

Fig. 9 Clinical case II with lung division

Table 3 Clinical case II: Parameter extraction. Reduced ventilation (RV) in regions 2, 3 and 7, and compensatory ventilation (CV) in regions 4 and 8

Signal	A	H	R
1	2.44	0.81	−0.129
2	2.98	0.74	−0.098
3	2.63	0.75	−0.133
4	15.94	0.76	−0.082
5	3.18	0.86	0.013
6	10.58	0.76	0.037
7	8.81	0.77	0.034
8	22.76	0.75	−0.023

It is abnormal that the updown ratios of the right lung are negative, while those of the left lung are almost all positive

- Case 2: A pathological case (see Fig. 9 and Table 3). By comparing this case with the previous normal case, it is clear that ventilation in regions 2 and 3 is poor. Ventilation amplitudes are expected to increase from region 1 to region 4 and from region 5 to region 8. Therefore, it is abnormal to observe an amplitude in region 7 smaller than region 6. It is also abnormal to observe negative updown ratios in the right lung and predominantly positive ratios in the left lung. Furthermore, regions

Table 4 Statistics of ventilation abnormalities with ROI-based analysis

Right/Left	NV	RV	ASV	NSV	CV
Apex(1/5)	0/0	4/5	25/19	23/17	0/1
Upper(2/6)	0/1	3/1	1/1	3/4	1/2
Mid(3/7)	2/0	9/4	5/3	11/3	0/1
Lower(4/8)	0/0	7/7	2/3	3/3	0/0

Table 5 Number of user interactions required to guarantee segmentation accuracy and robustness

	Seeds in first frame	User interactions in other frames
Max	5	2
Min	3	0
Average	3.3	0.3

4 and 8 are "hard" at work to compensate for the abnormal areas—the phenomena of "compensatory ventilation": an area with excessive ventilation in order to compensate for the abnormal areas in other parts of the lungs. This generally goes along with non-ventilation and reduced ventilation. The area itself should be considered as normal, but it is suggestive for abnormalities in other parts of the lungs. The HRCT report confirmed our findings in the right lung: bronchiectatic changes in the right middle and lower lobes, and scar changes in the right middle lobe medially. However, the report provided no explanation for the smaller amplitude of region 7 with respect to region 6.

The statistics of abnormal findings with our 53 ventilation patients are summarized in Tabel 4. Through the clinical cases studies, we have found that ROI-based ventilation analysis is efficient and effective with respect to the size of lung divisions. As the lung field is divided into finer regions, smaller ventilation irregularities are detected.

In the clinical studies, we also have found that United Snakes are not only efficient, providing real-time performance, but also accurate and require little user intervention. This performance is due, in part, to the use of the hard constraint mechanism offered by the United Snakes technique. The hard constraint at the lung apex plays a critical role by pinning the Snake—without it the snake would slide away from the lung apex. Furthermore, due to the interaction mechanisms provided by United Snakes, the segmentation and motion tracking can be made as accurate as desired by the user. The number of user interactions are given in Table 5, showing little user intervention is required.

5 Diaphragm Motion Analysis

The diaphragm is a dome-shaped sheet of muscle that separates the chest from the abdomen. As the diaphragm contracts and flattens, the volume of the chest increases and air is drawn into the lungs. As it relaxes, the dome pushes upward, forcing air out of the lungs. The diaphragm contracts without any voluntary control. During quiet breathing, there is no contraction of intercostal muscles. Therefore, analyzing the diaphragm motion gives first-hand information concerning pulmonary ventilation.

5.1 Quantifying Diaphragm Motion

Although we can extract diaphragm motion from the lung delineation result in Sect. 4, a more efficient quantitative analysis can be obtained using United Snakes. In the current patient orientation, the diaphragm is restricted to an up-and-down motion. Consequently, we use an open Snake and restrict its motion along the y-axis, leading to efficient tracking as only a few Snake nodes are required and only one deformation direction is needed for each node. The diaphragm motion can be characterized using the average position of the Snake over time.

5.2 Clinical Case Studies

Three clinical cases are presented:

- Case 1 (Fig. 10): A clinically normal case. The diaphragm moves freely and continuously.
- Case 2 (Fig. 11): Local abnormal diaphragm motion. The right diaphragm is expected to contract even further during inhalation, but it exhibits no observable motion for about half a second. Air is not effectively drawn into the right lung.
- Case 3 (Fig. 12): Global diaphragm motion abnormality. The left diaphragm cannot move freely and exhibits further irregularities during exhalation.

The number of user interactions needed for diaphragm motion analysis is minimal—only two seeds are required in the first frame to initialize a Snake, and no further user intervention is needed for any other frames due to the strong image contrast at the diaphragm. The abnormal diaphragm motion findings are summarized in Table 6.

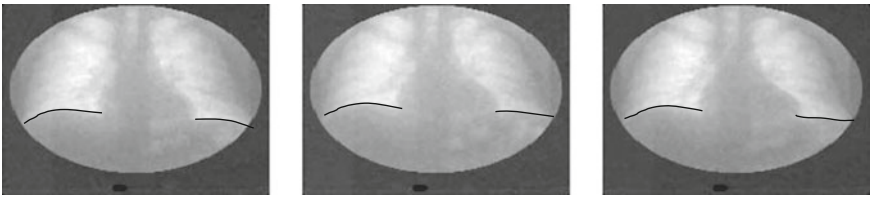

(a) Frame 5 (t=0.32) **(b)** Frame 15 (t=1.12) **(c)** Frame 25 (t=1.92)

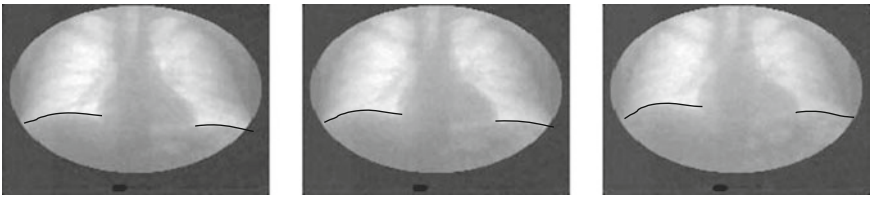

(d) Frame 35 (t=2.72) **(e)** Frame 45 (t=3.52) **(f)** Frame 55 (t=4.32)

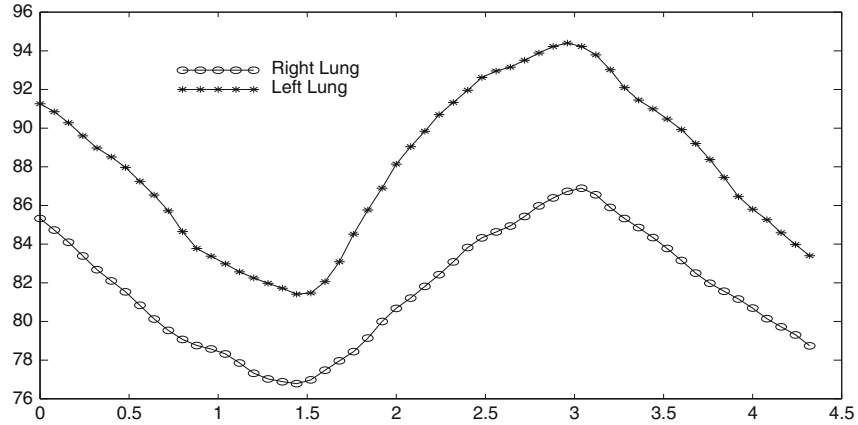

(g) Diaphragm Motion: Average y-positions of the two open snakes

Fig. 10 Clinical case I: Normal diaphragm motion. The diaphragm moves freely and continuously on both sides

6 Cardiac Motion Analysis

For effective perfusion analysis, it is essential to understand the cardiac function. Analyzing the cardiac motion gives the first-hand information concerning its function.

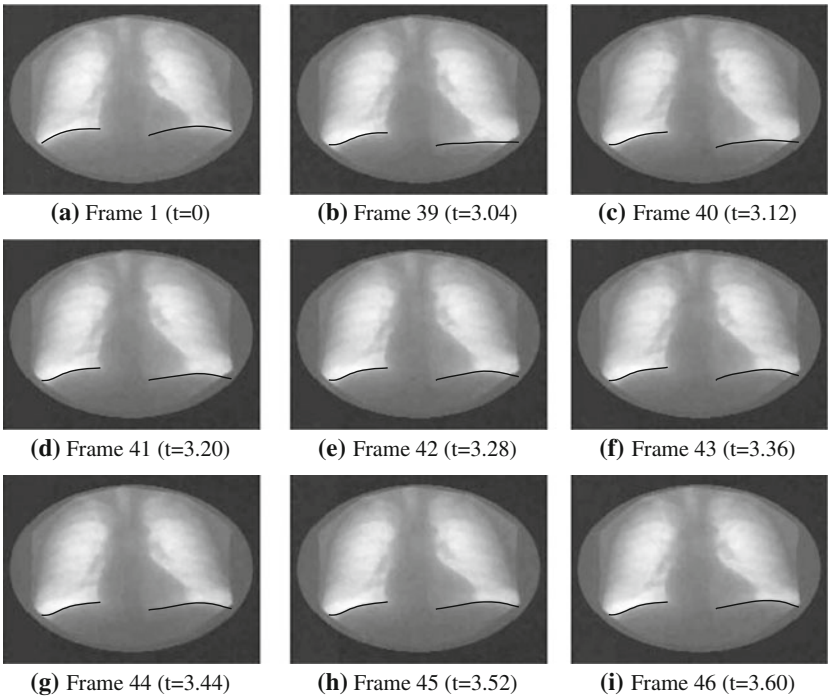

(a) Frame 1 (t=0) **(b)** Frame 39 (t=3.04) **(c)** Frame 40 (t=3.12)

(d) Frame 41 (t=3.20) **(e)** Frame 42 (t=3.28) **(f)** Frame 43 (t=3.36)

(g) Frame 44 (t=3.44) **(h)** Frame 45 (t=3.52) **(i)** Frame 46 (t=3.60)

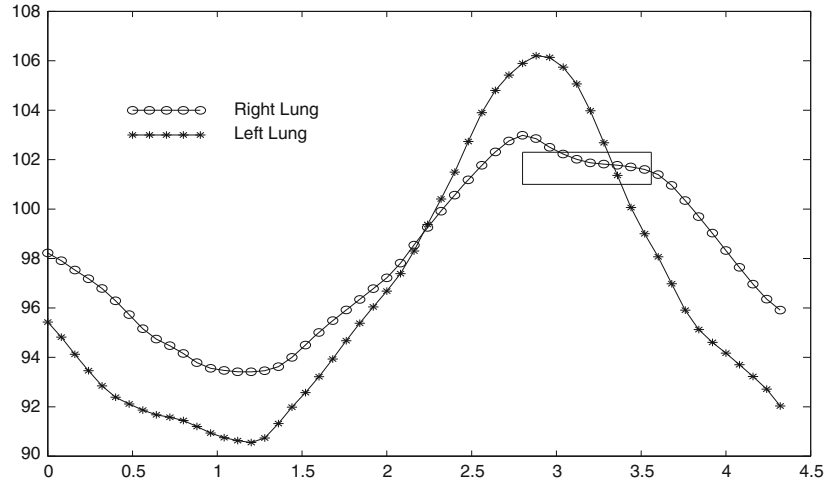

(j) Diaphragm Motion: Average y-positions of the two open snakes

Fig. 11 Clinical case II: Local abnormal diaphragm motion. **a** The two open snakes on the first frame. (**b**)–(**i**) From Frame 39 (t = 3.04) to Frame 46 (t = 3.60), the right diaphragm is expected to contract even further during inhalation, but it exhibits no observable motion (in term of pixels) for about half a second. **j** The average positions of the two open snakes. The local motion abnormality is indicated with a rectangle. The right diaphragm motion amplitude is also small

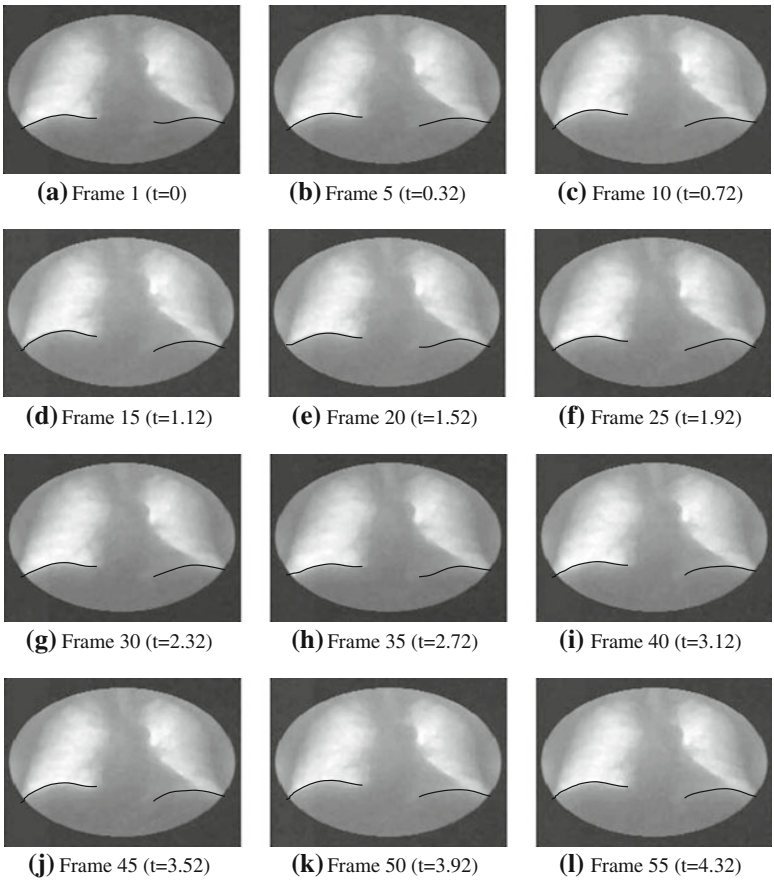

Fig. 12 Clinical case III: Global abnormal diaphragm motion. The left diaphragm cannot move freely and exhibits irregularities during exhalation

Table 6 Statistics of diaphragm motion abnormalities

	Global	Local
Right	4	11
Left	3	7

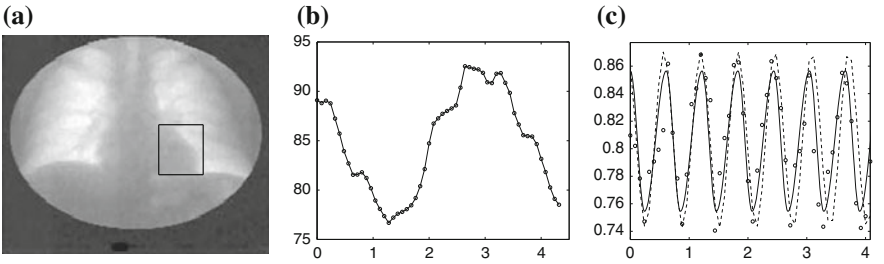

Fig. 13 **a** An ROI on the heart and **b** its corresponding observation. The observation is dominated by ventilation when the patient breathes. Our simple approach cannot extract the systolic and diastolic phases from such a signal. **c** However, with cardiac motion tracking (Fig. 15), the heart signal (indicated with "o") can be obtained with Eq. 8, and cardiac systolic and diastolic phases from the heart signal can be extracted with our perfusion model even when the patient breathes (the dashed curve indicates the initial guess and the final optimized result is shown with the solid curve)—the uptime corresponds to the diastolic phase (the heart proportion increases) and the downtime to the systolic phase of the heart (the heart proportion decreases). The extracted parameters for this patient are included in Table 7 as clinical case I, indicating that the heart is working properly

6.1 Characterizing Cardiac Motion

In order to use cardiac information to accelerate the pulmonary perfusion analysis, we proposed a simple approach to extract the cardiac systolic and diastolic phases from the heart [17]. We justify in Sect. 6.2 that this simple approach is sufficiently accurate for this purpose. However, it cannot be used to characterize complete cardiac motion for the following reasons:

- Its amplitude cannot be fully trusted in measuring the effectiveness of cardiac function. During perfusion examination, the patient is asked to hold their breath. The amount of air held in the lungs may differ from patient to patient and may differ from examination to examination, even for the same patient. As a result, when there is more air kept in the right lung, even if the heart doesn't pump effectively we may still have a higher amplitude due to the higher contrast along the cardiac boundary.
- This simple approach does not work when ventilation is present. When the patient breathes, the signal will be dominated by ventilation as shown in Fig. 13. Therefore, it cannot extract the systolic and diastolic phases from such a signal.

United Snakes offers a general solution for characterizing cardiac motion. By tracking cardiac motion (see Fig. 14), the heart proportion in an ROI can be computed

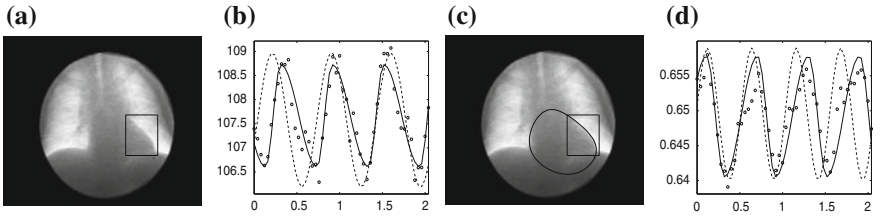

Fig. 14 Clinical case IV: Extracting cardiac motion parameters (with the same notation as in Fig. 16)

Table 7 Cardiac motion parameters given by our general approach for the four clinical cases

Clinical cases	Our new approach				
	A (amplitude %)	D (systolic)	U (diastolic)	S (timeshift)	F (frequency)
I	5.10	0.2398	0.3698	0.6106	98
II	2.40	0.3869	0.7931	0.9252	51
III	2.93	0.2065	0.9277	0.2144	53
IV	0.86	0.2106	0.3869	0.1105	100

The downtime (D) corresponds to the systolic phase, while the uptime (U) corresponds to the diastolic phase. The amplitude parameters show that the heart of Case I (a clinically normal case) is pumping effectively, while the heart pumping of Case IV (with advanced pulmonary embolism) is extremely weak. Cases II and III (both athletes) represent the typical "ineffective" phenomena of athletic hearts during rest: Low amplitude and low frequency

over time throughout the entire sequence resulting in a heart signal:

$$s_h = \frac{|\text{intersection of heart and ROI}|}{|\text{ROI}|}. \tag{8}$$

Analyzing the heart signal reveals the condition of cardiac function.

6.2 Clinical Case Studies

Clinical studies show that the new approach is effective in detecting abnormal cardiac function. We have applied this new approach to all of our clinical cases (53 ventilation patients and the 52 perfusion cases). We found weak cardiac function in 16 patients. Included here are three representative cases. Their results are listed in Table 7 and shown in Figs. 15, 16 and 17 as clinical cases II, III and IV. The amplitude parameters show the effectiveness of heart pumping action. According to our experiments, we expect that the amplitude of a healthy person is greater than 5.0 % (with the exception of athletes). Case I is a clinically normal case and the heart is pumping effectively. The heart pumping action of Case IV (with advanced pulmonary embolism) is extremely

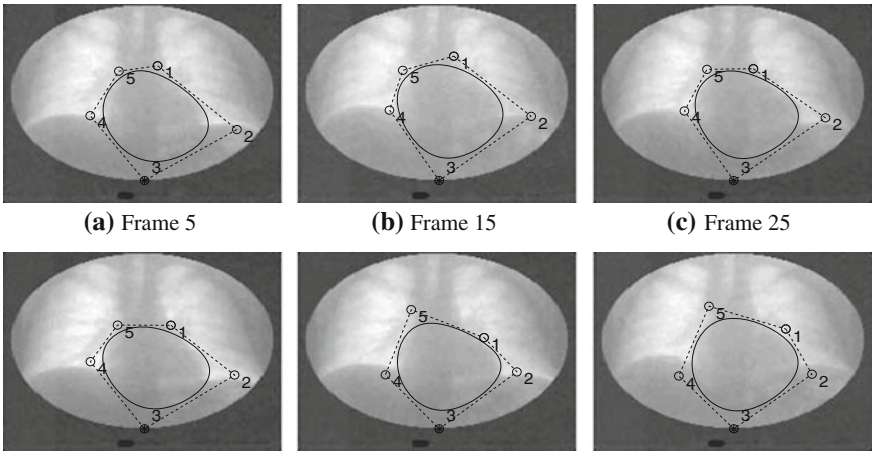

(a) Frame 5 **(b)** Frame 15 **(c)** Frame 25

(d) Frame 35 **(e)** Frame 45 **(f)** Frame 55

Fig. 15 A united snake with B-spline shape functions (noise insensitive) is used to track cardiac motion (every tenth image shown). The dashed polygon is the B-spline control polygon. To effectively bridge the gap along the heart boundary, a hard constraint is further imposed on control polygon node 3. The robust tracking performance is largely due to the hard constraint

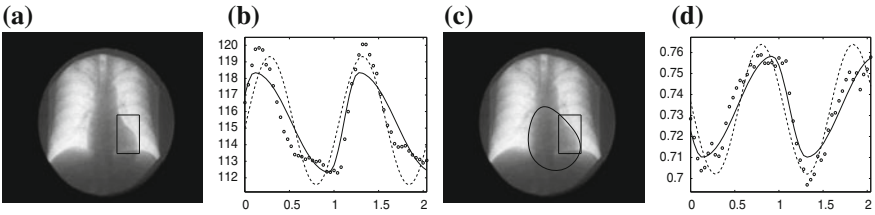

Fig. 16 Clinical case II: Extracting cardiac motion parameters with our previous, simple approach used for perfusion analysis in [17] (**a**, **b**) and the more general approach (**c**,**d**). The observations are indicated with "o", the initial guesses with the dashed curves and the final optimized results with the solid curves. The numerical results are given in Tables 8 and 7, respectively

ineffective. Cases II and III are both athletes representing the typical "ineffective" phenomena of athletic hearts during rest (low amplitude and slow cardiac rate).

The cardiac motion tracking approach can be used to justify the accuracy of our previous approach in [17]. By comparing the results given by our previous approach (see Table 8) and by the motion tracking approach (see Table 7), the absolute differences of the systolic/diastolic phases are less than 0.08 s. This means that our previous approach is a simple, fast, and accurate technique for extracting the systolic and diastolic phases from the heart.

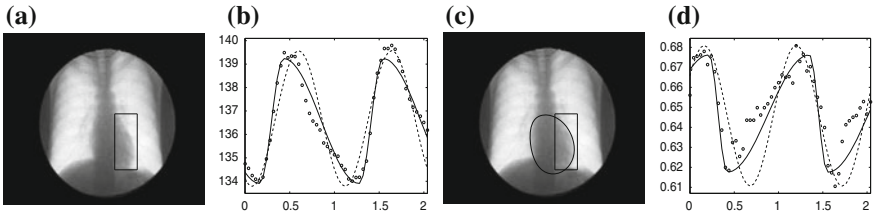

Fig. 17 Clinical case III: Extracting cardiac motion parameters (with the same notation as in Fig. 16)

Table 8 Cardiac motion parameters given by our previous approach

Clinical cases	Our previous approach			
	D (diastolic)	U (systolic)	S (timeshift)	F (frequency)
I	N/A	N/A	N/A	N/A
II	0.8361	0.3366	0.1067	51
III	0.8473	0.2658	0.4301	53
IV	0.4250	0.1770	0.3112	100

The method does not work when ventilation is present (Case I). The amplitude is not included, since it does not have a well-defined medical meaning. The uptime (U) for the systolic phase and the downtime (D) for the diastolic phase. The uptime and downtime in this table have completely different medical meanings from those in Table 7. Comparing with Table 7, the maximal absolute difference in systolic/diastolic phases is 0.08 s. Therefore, the simple approach is sufficiently accurate for extracting the systolic and diastolic phases and safe for perfusion analysis in [17]

7 Cardiac Shape Analysis

7.1 Revised Cardiothoracic Ratio (RCTR)

Cardiac size is an important and useful diagnostic parameter in chest radiographs. The conventional measurement for assessing cardiac enlargement is the cardiothoracic ratio (CTR) [18, 19]. Referring to Fig. 18, the CTR is defined as the ratio of the transverse diameter of the cardiac shadow to the greatest transverse diameter of the thorax [20] or the transverse diameter of the thorax at the highest level of the diaphragm [21]. Many researchers have reported the relationship between cardiac disease and heart size, and demonstrated the usefulness of the CTR and estimated cardiac size in clinical applications (e.g., [22–29]). Several research groups have attempted the automatic calculation of cardiac parameters for diagnosis [30–36].

However, the CTR is generally calculated from a single chest radiograph in which the heart may be in any phase of motion and, consequently, it is subject to measurement errors. In Dynamic Pulmonary Imaging, a whole cardiac motion cycle is available and the minimal CTR and maximal CTR may be computed to form an interval as a revised measurement of cardiac size. That is,

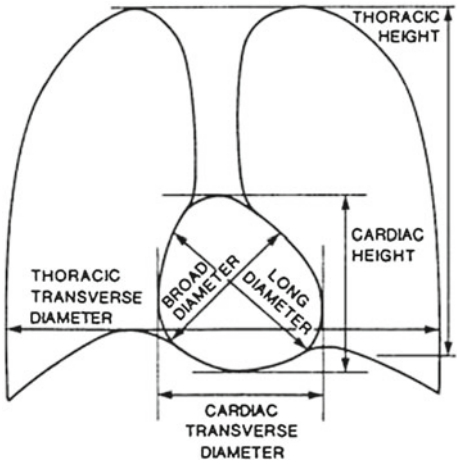

Fig. 18 Various parameters of the heart and lungs in chest radiographs given by Nakamori et. al. in [36]. "Cardiac broad diameter" may also be referred as "cardiac short diameter"

$$CTR_{min} = \frac{\min_t C(t)}{\max_t T(t)} \tag{9}$$

$$CTR_{max} = \frac{\max_t C(t)}{\max_t T(t)} \tag{10}$$

where $C(t)$ is the transverse diameter of the cardiac shadow at time t and $T(t)$ is the transverse diameter of the thorax at time t. The difference between CTR_{min} and CTR_{max} indicates the strength (effectiveness) of the heart pumping action. For a normal case, we expect that $CTR_{min} < CTR_{max} \leq 50\,\%$ and $CTR_{max} - CTR_{min} > 5\,\%$ with the exception of athletes.

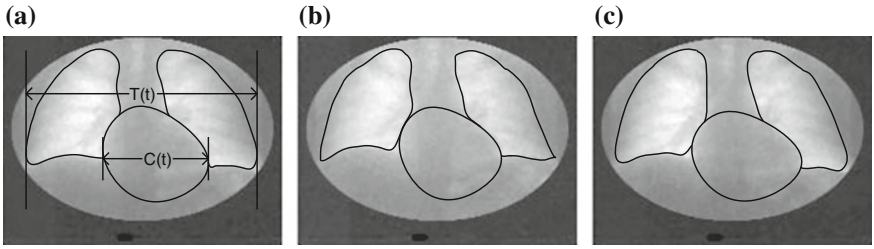

Fig. 19 Case I (with ventilation): Calculating RCTR. **a** The maximal thoracic transverse diameter (i.e., $max_t(T(t))$). **b** The minimal cardiac transverse diameter (i.e., $min_t(C(t))$). **c** The maximal cardiac transverse diameter (i.e., $max_t(C(t))$). A clinically normal case with normal heart size and effective heart pumping

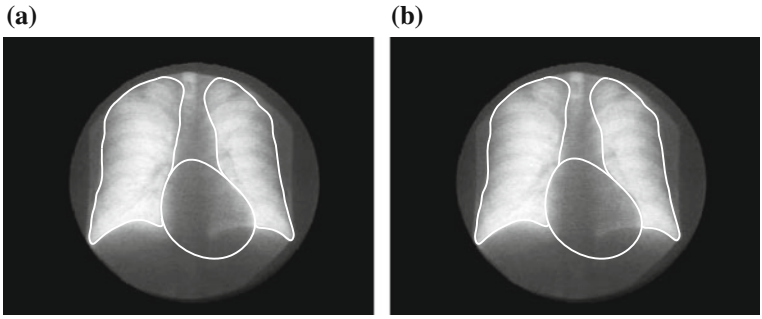

Fig. 20 Case II (with the breath held): **a** The minimal cardiac transverse diameter. **b** The maximal cardiac transverse diameter. The thoracic transverse diameter is a constant over time due to the held breath. An athlete. Heart size is normal, but heart pumping is weak. This is the typical "ineffective" phenomena of athletic hearts during rest

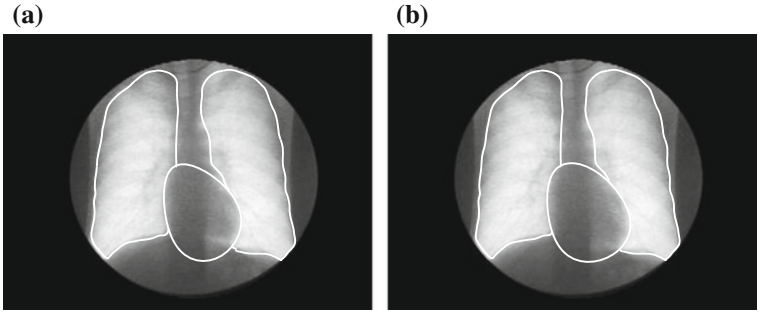

Fig. 21 Case III (with the breath held): Another athlete with the typical phenomena of athletic hearts during rest. The same notation is used as in Fig. 20

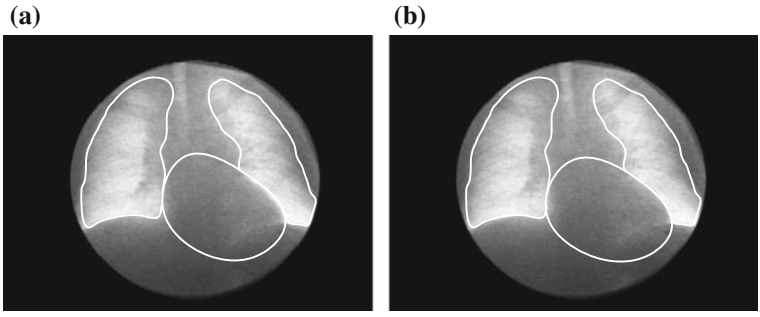

Fig. 22 Case IV (with the breath held): Calculating RCTR. **a** The minimal cardiac transverse diameter. **b** The maximal cardiac transverse diameter. The thoracic transverse diameter is a constant over time due to the breath held. A pathological case with advanced pulmonary embolism. Large heart and extremely ineffective heart pumping action

7.2 Clinical Case Studies

We have applied this new measurement to our 53 ventilation patients and 52 perfusion patients. We have found that 7 of them have large hearts and heart pumping is not effective in 16 cases. Here we list four representative cases:

- **Case I (with ventilation)** (see Fig. 19): A clinically normal case. Normal heart size and effective heart pumping ($CTR_{min} = 40.22\,\%$ and $CTR_{max} = 46.53\,\%$).
- **Case II** (see Fig. 20): An athlete. Heart size is normal, but heart pumping is weaker ($CTR_{min} = 45.97\,\%$ and $CTR_{max} = 47.29\,\%$) than Case I. This is the typical "ineffective" phenomena of athletic hearts
- **Case III** (see Fig. 21): Another athlete. Heart size is good but it does not pump as effectively ($CTR_{min} = 37.99\,\%$ and $CTR_{max} = 40.92\,\%$) as Case I. Again, the typical phenomena of athletic hearts during rest.
- **Case IV** (see Fig. 22): This is a pathological case with advanced pulmonary embolism. Large heart and extremely ineffective heart pumping ($CTR_{min} = 53.49\,\%$ and $CTR_{max} = 54.38\,\%$).

These patients are the same as in Sect. 6.2. Referring to Table 7, we can see that the findings there are corroborated by the new findings here.

8 Conclusions

This chapter has utilized our United Snakes technique to reveal pulmonary ventilation and perfusion abnormalities through motion and shape analysis of the lungs and heart. This fluoroscopical examination takes only about 4 s for ventilation studies and 2 s for perfusion studies with low radiation dose to the patient and with no preparation, radioactive isotopes, and contrast media.

References

1. Kiuru A, Svedstrom E (2003) Method to measure the relative perfusion of the lungs. U.S. Patent US 6,522,720 B1, 28 Feb 2003
2. Levenberg K (1944) A method for the solution of certain problems in least squares. Quart Appl Math 2:164–168
3. Marquardt DW (1963) An algorithm for least-squares estimation of nonlinear parameters. SIAM J Appl Math 11:431–441
4. Scales LE (1985) Introduction to non-linear optimization. Macmillan Publishers Ltd, New York
5. Kass M, Witkin A, Terzopoulos D (1988) Snakes: active contour models. Int J Comput Vision 1(4):321–331
6. McInerney T, Terzopoulos D (1996) Deformable models in medical image analysis: a survey. Med Image Anal 1(2):91–108

7. Singh A, Goldgof D, Terzopoulos D (eds) (1998) Deformable models in medical image analysis. IEEE Computer Society Press, Los Alamitos
8. Blake A, Isard M (1998) Active contours. Springer-Verlag, New York
9. Mortensen EN, Barrett WA (1995) Intelligent scissors for image composition. In: Proceedings of computer graphics (SIGGRAPH'95), Los Angeles, CA, Aug 1995, pp 191–198
10. Barrett W, Mortensen E (1997) Interactive live-wire boundary extraction. Med Image Anal 1(4):331–341
11. Mortensen EN, Barrett WA (1998) Interactive segmentation with intelligent scissors. Grap Models Image Process 60:349–384
12. Falcão AX, Udupa JK, Samarasekera S, Hirsch BE (1996) User-steered image boundary segmentation. In: Proceedings of SPIE on medical imaging, vol. 2710, Newport Beach, CA, 1996, pp 278–288
13. Falcão AX, Udupa JK (1997) Segmentation of 3D objects using livewire. In: SPIE on medical imaging 1997, vol 3034, Newport Beach, CA, 1997, pp 228–239
14. Falcão AX, Udupa JK, Samarasekera S, Sharma S (1998) User-steered image segmentation paradigms: live wire and live lane. Grap Models Image Process 60:233–260
15. Falcão AX, Udupa JK, Miyazawa FK, An ultra-fast user-steered segmentation paradigm: Live-wire-on-the-fly. IEEE Trans Med Imaging (to appear)
16. Liang J, McInerney T, Terzopoulos D (2006) United snakes. Med Image Anal 10(2):33–215
17. Liang J, Järvi T, Kiuru A, Kormano M, Svedström E (2003) Dynamic chest image analysis: model-based perfusion analysis in dynamic pulmonary imaging. EURASIP J Appl Sig Process 2003(5):437–448 (Special Issue on Advances in Modality-Oriented Medical Image Processing)
18. Burgener FA, Kormano M (1991) Differential diagnosis in conventional radiology. Thieme, Stuttgart
19. Sutton D (1987) A textbook of radiology and imaging. Churchill Livingston, New York
20. Shanks SC, Kerley P (1962) A text-book X-ray diagnosis. Saunders, Philadelphia
21. Cooley RN, Schreiber MH (1978) Radiology of the heart and great vessels. William and Wilkins, Baltimore
22. Fuster V, Gersh BJ, Giuliani ER, Tajik AJ, Brandenburg RO, Frye RL (1981) The natural history of idiopathic dilated cardiomyopathy. Am J Cardio 47:525–531
23. Hutsebaut J, Scano G, Garcia-Herreros P, Degre S, DeCoster A, Sergysels R (1981) Hemodynamic characteristics in chronic obstructive lung diseases as related to cardiac size. Respiration 41:25–32
24. Gomez GA, Park JJ, Panahon AM, Pathasarathy KL, Pearce J, Reese P, Bakshi S, Henderson ES (1983) Heart size and function after radiation therapy to the mediastinum in patients with Hoggkin's disease. Cancer Threat Rep 67:1099–1103
25. Edwards DK, Higgins CB, Gilpin EA (1981) The cardiothoracic ratio in newborn infants. Am J Radiol 136:907–913
26. Kortman KE, Edwards DK, Deutsch AL, Higgins CB (1984) Heart size in newborn infants with birth asphyxia. Am J Radiol 143:533–535
27. Lauder IJ, Milns JS (1976) Longitudinal study of heart size in older people. Br Heart J 38:1286–1290
28. Nickol K, Wade AJ (1982) Radiographic heart size and cardiothoracic ratio in three ethnic groups: a basis for a simple screening test for cardiac enlargement in men. Br Heart J 55:399–403
29. Kabala JE, Wilde P (1987) The measurement of heart size in the anteroposterior chest radiograph. Br J Radiol 60:981–986
30. Myers PH, Nice CM, Becker HC, Nettleton WJ, Sweeney JW, Mechstroth GR (1964) Automated computer analysis of radiographic images. Radiology 83:1029–1033
31. Becker HC, Nettleton WJ, Myers PH, Sweeney JW, Mechstroth GR, Nice CM (1964) Digital computer determination of a medical diagnostic index directly from chest X-ray images. IEEE Trans Biomed Eng 11:67–72
32. Hall DH, Lodwick GS, Kruger RP, Dwyer SJ, Townes JR (1971) Direct computer diagnosis of rheumatic heart disease. Radiology 101:497–509

33. Kruger RP, Townes JR, Hall DL, Dwyer SJ, Lodwick GS (1972) Automated radiographic diagnosis via feature extraction and classification of cardiac size and shape desecrators. IEEE Trans Biomed Eng 19:174–186
34. Sezaki N, Ukena K (1973) Automatic computation of the cardiothoracic ratio with application to mass screening. IEEE Trans Biomed Eng 20:248–253
35. Paul JL, Levine MD, Fraser RG, Laszlo CA (1973) Automatic. IEEE Trans Biomed Eng 20:248–253
36. Nakamori N, Doi K, Sabeti V, MacMahon H (1990) Image feature analysis and computer-aided diagnosis in digital radiography: Automated analysis of sizes of heart and lung in chest images. Medl Phys 17(3):342–350